PROCEEDINGS, 44th Workshop on Geothermal Reservoir Engineering
Stanford University, Stanford, California, February 11-13, 2019
SGP-TR-214

Adaptive Viscoelastic-Waveform Inversion Using the Local Wavelet Transform for Geothermal Reservoir Characterization at the Blue Mountain Geothermal Field

Wenyong Pan and Lianjie Huang

Los Alamos National Laboratory, Geophysics Group, MS D452, Los Alamos, NM 87545, USA

wenyongp@lanl.gov; ljh@lanl.gov

Keywords: Attenuation, Blue Mountain, geothermal reservoir, viscoelastic-waveform inversion, wavelet transform

ABSTRACT

Seismic attenuation is a key parameter for geothermal reservoir characterization. Viscoelastic-waveform inversion has potential to reconstruct both subsurface velocities and attenuation coefficients. However, the strong trade-offs between velocity and attenuation parameters make it difficult to invert for the attenuation parameters reliably. We develop a novel adaptive viscoelastic-waveform inversion method based on the local wavelet transform for velocity and attenuation inversion. We first use a multi-scale elastic-waveform inversion scheme to invert for the velocity models, and then employ a spectral amplitude-ratio misfit function based on the local wavelet transform of seismic traces for attenuation inversion. We verify the method using synthetic seismic data, and validate it using a field seismic dataset acquired at the Blue Mountain geothermal field. Our preliminary results demonstrate that the regions with high-attenuation coefficients may be associated with fluid-filled fracture/fault zones in geothermal reservoirs.

1. INTRODUCTION

The Blue Mountain geothermal field (Figure 1), located in northern Nevada, has been in operation since November 2009. However, the resources experienced significant temperature decrease because of reinjection into wells on the west side of the field. Since 2013, all but one of the western injectors have been idle, with reinjection moved to the northern and northeastern edges of the field. Wells on the southern edge of the field, where new reinjection could mine significant stranded heat-in-place, remain idle because of low permeability. Former injection wells at the western edge of the field were initially very hot but they may not re-heat to pre-injection temperatures. Thus, new hot production wells at the western edge of the field may be needed to bring the plant production back up to initial production. Identifying the locations of the subsurface geothermal reservoirs accurately is essential for optimizing well placement of new injection/production wells.

Figure 1: The Blue Mountain geothermal field in Nevada

In recent decades, seismic waveform inversion has emerged as a powerful technique to obtain high-resolution subsurface velocity models for improving the accuracy of seismic imaging (Tarantola, 1984; Virieux and Operto, 2009). Seismic waveform inversion minimizes the differences between observed seismic data and synthetic data. When seismic waves propagate in Earth, seismic waveforms suffer from amplitude decay and velocity dispersion caused by seismic attenuation. Subsurface attenuation models are critical for compensating the amplitude and phase distortions in seismic imaging and provide independent constraints on the rock/fluid properties of the reservoir target. Seismic waveform inversion holds the ability of obtaining subsurface elastic and attenuation properties for reservoir characterization. However, simultaneously determining velocity and attenuation models using waveform inversion introduces the problem of interparameter trade-off, that is, smaller velocity errors may have strong influences to the inverted attenuation models.

In this paper, we develop a novel adaptive viscoelastic-waveform inversion method based on the local wavelet transform and spectral amplitude-ratio (SAR) misfit function for obtaining subsurface velocity and attenuation models. The forward modeling problem in

viscoelastic media is solved using the generalized standard linear solid (GSLS) model (Carcione et al., 1988; Robertsson et al., 1994). A two-stage approach is designed for reconstructing velocity and attenuation models separately. In Stage I, we use traditional waveform-difference (WD) misfit function to invert for improved velocity models. This stage minimizes the phase residuals in seismic data. In Stage II, we invert for attenuation models using the SAR misfit function and the local wavelet transform. Load time windows are designed to separate early arrivals and reflections in seismic data. The local amplitude residuals obtained from the local wavelet transform are minimized by updating the attenuation models. The SAR misfit function shows stronger sensitivity to the attenuation anomalies than other misfit functions, and is able to invert for attenuation models more reliably and efficiently.

An active seismic survey along seven 2D lines was carried out at the Blue Mountain geothermal field in 2007 for subsurface characterization (Optim, 2007). Optim built a tomography velocity model using refraction tomography and conducted prestack Kirchhoff depth migration for each line of seismic data. Kirchhoff migration is based on ray theory. Huang et al., (2018) applied anisotropic full-waveform inversion and least-squares reverse-time migration to the surface seismic data acquired along seven lines at the Blue Mountain geothermal field and obtained improved velocity models and migration images.

In this paper, we apply our new adaptive viscoelastic-waveform inversion method to the seismic data acquired along Line 3, and obtain high-resolution velocity and attenuation models. In the inverted attenuation models, we observe strong attenuation anomalies, which may be associated with fluid-filled fracture/fault zones in geothermal reservoirs, demonstrating that our attenuation inversion results can provide informative references for optimizing well placement of new injection/production wells.

The paper is organized as follows. We first describe forward modeling problem in viscoelastic media of the GSLS model, and then the theory of adaptive viscoelastic-waveform inversion method based on the spectral amplitude-ratio misfit function and the local wavelet transform for velocity and attenuation estimation. In the numerical modeling section, we first carry out synthetic experiment to verify the effectiveness of our new method. We then apply our new method to the surface seismic data acquired from the Blue Mountain geothermal field data.

2. METHODOLOGY

2.1 Forward Modeling in Viscoelastic Media

We simulate the wave propagation in viscoelastic media based on the common generalized standard linear solid (GSLS) model (Carcione et al., 1988; Robertsson et al., 1994). In a linear anisotropic viscoelastic medium, the wave equation is given by

$$\rho(x)\ddot{u}_i(x,t)+\partial_j\left[\int_0^t c_{ijkl}(x,t-t^{"})\dot{\varepsilon}_{kl}(x,t^{"})dt^{"}\right]=f_i(x_s), \tag{1}$$

where ρ is the mass density, u_i is the i th component of the displacement field, the symbol " ¨ " means the second-order time derivative, f_i is the source term, $\dot{\varepsilon}_{kl}$ is the first-order time derivative of the strain field and c_{ijkl} is the relaxation function. In isotropic viscoelastic media, the relaxation function can be written as:

$$c_{ijkl}(x,t)=\left[\kappa^R(x,+\infty)\delta_{ij}\delta_{kl}+\mu^R(x,+\infty)\left(\delta_{ik}\delta_{jl}+\delta_{il}\delta_{jk}-\frac{2}{3}\delta_{ij}\delta_{kl}\right)\right]\left[1+\frac{1}{P}\sum_{p=1}^{P}\tau_{ijkl}\exp\left(-\frac{t}{\tau^{\sigma p}}\right)\right]H(t), \tag{2}$$

where κ^R and μ^R are the relaxed bulk modulus and shear modulus, respectively, δ is the Dirac delta function, P is the maximum number of relaxation mechanisms, H is the Heaviside function ensuring the causality, and τ_{ijkl} determines the magnitude of the attenuation level. The inconvenient convolution in the constitutive relation can be eliminated by taking time derivative of the stress tensor:

$$\dot{\sigma}_{ij}(x,t)=\left[\kappa^R(x,+\infty)\delta_{ij}\delta_{kl}+\mu^R(x,+\infty)\left(\delta_{ik}\delta_{jl}+\delta_{il}\delta_{jk}-\frac{2}{3}\delta_{ij}\delta_{kl}\right)\right]\left[\left(\tau_{ijkl}+1\right)\dot{\varepsilon}_{kl}(x,t)-\tau_{ijkl}\frac{1}{P}\sum_{p=1}^{P}\dot{\tilde{\varepsilon}}_{kl}^{p}(x,t)\right], \tag{3}$$

where $\tilde{\varepsilon}_{kl}^{p}$ are the memory strain variables:

$$\tilde{\varepsilon}_{kl}^{p}(x,t)=\frac{1}{P\tau^{\sigma p}}\int_0^t\exp\left(-\frac{t-t^{"}}{\tau^{\sigma p}}\right)H\left(t-t^{"}\right)\dot{\varepsilon}_{kl}(x,t^{"})dt^{"}, \tag{4}$$

satisfying the following partial differential equation:

$$\dot{\tilde{\varepsilon}}_{kl}^{p}(x,t)=-\frac{1}{\tau^{\sigma p}}\dot{\varepsilon}_{kl}^{p}(x,t)+\frac{1}{P\tau^{\sigma p}}\dot{\varepsilon}_{kl}(x,t). \tag{5}$$

Thus, the convolution constitutive relation can be replaced by solving a set of partial differential equations. Based on the superposition of relaxation mechanisms, the linear viscoelasticity formations allow us to simulate wave propagation in attenuative media with arbitrary spatial distributions of the quality factors.

2.2 Viscoelastic-Waveform Inversion

Seismic waveform inversion methods estimate model properties iteratively by minimizing the differences between observed data u_i^{obs} and synthetic data u_i, which gives the following waveform-difference (WD) misfit function:

$$\chi^{WD}(m)=\frac{1}{2}\sum_{x_r}\int_0^{t'}\left[u_i(x_r,t;m)-u_i^{obs}(x_r,t)\right]^2 dt, \tag{6}$$

where m and t' indicate the model parameter and the maximum recording time, respectively. Variations of the misfit function with respect to the perturbations of ρ, κ and μ give the following sensitivity kernels:

$$\begin{aligned}
K_\rho &= -u_i^\dagger \ddot{u}_i,\\
K_\kappa &= -\left(\kappa * \dot{\varepsilon}_{ii}^\dagger\right)\varepsilon_{kk},\\
K_\mu &= -\left[\left(\delta_{ik}\delta_{jl}+\delta_{il}\delta_{jk}-\frac{2}{3}\delta_{ij}\delta_{kl}\right)\mu * \dot{\varepsilon}_{ij}^\dagger\right]\varepsilon_{kl},
\end{aligned} \tag{7}$$

According the relationship between the modulus parameters and the corresponding modulus quality factors (Q_κ and Q_μ), the sensitivity kernels of the modulus quality factors are given by

$$K_{Q_\kappa}=-\frac{K_\kappa^{Q_\kappa}}{Q_\kappa}, K_{Q_\mu}=-\frac{K_\mu^{Q_\mu}}{Q_\mu}, \tag{8}$$

where the expressions of kernels $K_\kappa^{Q_\kappa}$ and $K_\mu^{Q_\mu}$ are the same with K_κ and K_μ but invoking different adjoint source $f_{i,Q}^\dagger$:

$$f_{i,Q}^\dagger(x,t)=\frac{1}{2\pi}\int_{-\infty}^{+\infty}\left[\frac{2}{\pi}\ln\frac{|\omega|}{\omega_0}-\mathbf{i}\,\mathrm{sign}(\omega)\right]\tilde{f}_{i,WD}^\dagger(x,\omega)\exp(\mathbf{i}\omega t)d\omega, \tag{9}$$

where $\tilde{f}_{i,WD}^\dagger$ is the Fourier transform of the regular adjoint source for the WD misfit function. The linear viscoelastic media is commonly described using P-wave velocity α, S-wave velocity β, P-wave velocity quality factor Q_α and S-wave velocity quality factor Q_β. The corresponding sensitivity kernels are given by

$$\begin{aligned}
K_\alpha &= 2\left(1+\frac{4\beta^2}{3\alpha^2-4\beta^2}\right)K_\kappa+\left(\frac{2\alpha^2}{\alpha^2-\beta^2}-\frac{2\alpha^2Q_\beta}{\alpha^2Q_\beta-\beta^2Q_\alpha}\right)K_{Q_\kappa},\\
K_\beta &= 2\left(K_\mu-\frac{4\beta^2}{3\alpha^2-4\beta^2}K_\kappa\right)+\left(\frac{2\beta^2Q_\alpha}{\alpha^2Q_\beta-\beta^2Q_\alpha}-\frac{\beta^2}{\alpha^2-\beta^2}\right)K_{Q_\kappa},\\
K_{Q_\alpha} &= \left(\frac{\alpha^2}{\alpha^2-\beta^2}+\frac{\beta^2Q_\alpha}{\alpha^2Q_\beta-\beta^2Q_\alpha}\right)K_{Q_\kappa},\\
K_{Q_\alpha} &= K_{Q_\mu}.
\end{aligned} \tag{10}$$

The L-BFGS method is used to construct the search direction for model updating at each nonlinear iteration.

Seismic attenuation leads to amplitude and phase distortions of seismic data. However, traveltime, and, at moderate frequencies, the phase, of seismic data are mainly controlled by velocity perturbations. The influence of attenuation is more pronounced on seismic amplitudes. For this reason, we design a new adaptive viscoelastic-waveform inversion strategy based on the local wavelet transform. In Stage I, the conventional WD misfit function is used to estimate velocity models, minimizing the phase residuals in seismic data. In Stage II, a new amplitude-based misfit function is used to estimate the attenuation models, minimizing the local spectral amplitude residuals in the local wavelet transform domain.

2.1.1 Spectral Amplitude-Ratio Misfit Function

We use the spectral amplitude-ratio (SAR) misfit function to estimate the attenuation models in Stage II, because the phase information is naturally separated from the amplitude information in the frequency domain. Thus, the SAR misfit function shows stronger sensitivity to attenuation anomalies than other misfit functions and is expected to invert for the attenuation models more reliably and efficiently. The SAR misfit function is defined as:

$$\chi^{SAR}(m)=\frac{1}{2}\sum_{x_r}\int_0^{\omega}\left[\ln\frac{A_i^{obs}(x_r,\omega)}{A_i(x_r,\omega)}\right]^2 dt, \tag{11}$$

where A_i is the amplitude spectrum of the seismic data. The regular adjoint source of this misfit function is given by

$$\tilde{f}^{\dagger}_{i,SAR}(x,\omega)=-\sum_{x_r}\ln\left[\frac{A_i^{obs}(x_r,\omega)}{A_i(x_r,\omega)}\right]\frac{u_i^{\dagger\dagger}(x_r,\omega;m)}{A_i^2(x_r,\omega;m)}\delta(x-x_r), \tag{12}$$

where $\dagger\dagger$ denotes the complex conjugate. The adjoint source for calculating the attenuation sensitivity kernels can be obtained by inserting equation (12) in equation (9).

2.1.2 Local Wavelet Transform

Wavelet transform of a seismic trace $u_i(t)$ is:

$$W(a,b)=\frac{1}{\sqrt{|a|}}\int_{-\infty}^{+\infty}u_i(t)\psi^{\dagger\dagger}\left(\frac{t-b}{a}\right)dt, \tag{13}$$

where $\psi(t)$ is a wavelet function, a and b are the scale and translation parameters. Compared to conventional Fourier transform, wavelet transform can describe the local features of seismic data in the space and frequency domains. Spectral amplitude variations within local time windows and specific frequency bands can be measured using local wavelet transform.

3. RESULTS

3.1 Synthetic Example

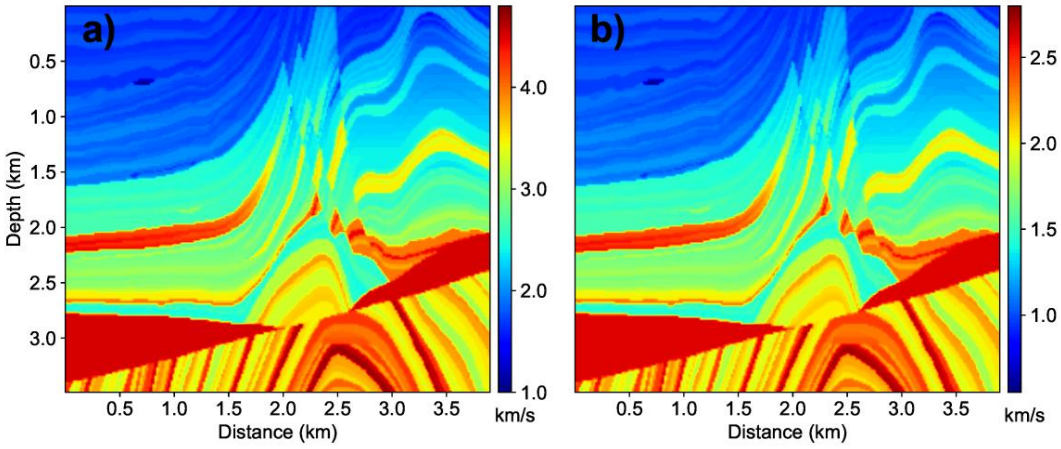

Figure 2: The true P-wave velocity α model (a) and S-wave velocity β model (b) used for testing our adaptive viscoelastic-waveform inversion method.

We first carry out synthetic inversion experiments to examine the effectiveness of our new adaptive viscoelastic-waveform inversion method. Figures 2a and 2b show the true P-wave velocity α and S-wave velocity β models used for our numerical test. The model dimension is 3.5 km in depth and 3.8 km in the lateral direction. Figures 3a and 3b display the true P-wave velocity quality factor Q_α and S-wave velocity quality factor Q_β models. The attenuation anomalies are embedded in the shallow parts of the homogeneous background. The initial α and β models used for inversion are shown in Figures 4a and 4b. The initial attenuation models are homogeneous with $Q_\alpha = Q_\beta = 150$.

In Stage I, we first invert for the P-wave and S-wave velocity models using the conventional WD misfit function, as shown in Figures 5a and 5b. High-resolution velocity structures are resolved. However, there are still some errors between the true models and inverted models, which may have strong influences on attenuation inversion. In Stage II, we use WD and SAR misfit functions to invert for the attenuation models. Figures 6a and 6b are the inverted Q_α and Q_β models using the WD misfit function, which are contaminated by very strong

parameter crosstalk artifacts. Only weak attenuation anomalies are recovered. The inverted Q_α and Q_β models by SAR misfit function contain few artifacts, as shown in Figures 7a and 7b. The recovered attenuation anomalies are very clear. Compared with WD misfit function, the data misfit of SAR misfit function also reduces faster in the process of attenuation inversion, as depicted in Figure 8. Our test on synthetic data demonstrate that our adaptive viscoelastic-waveform inversion can reliably reconstruct velocity and attenuation models.

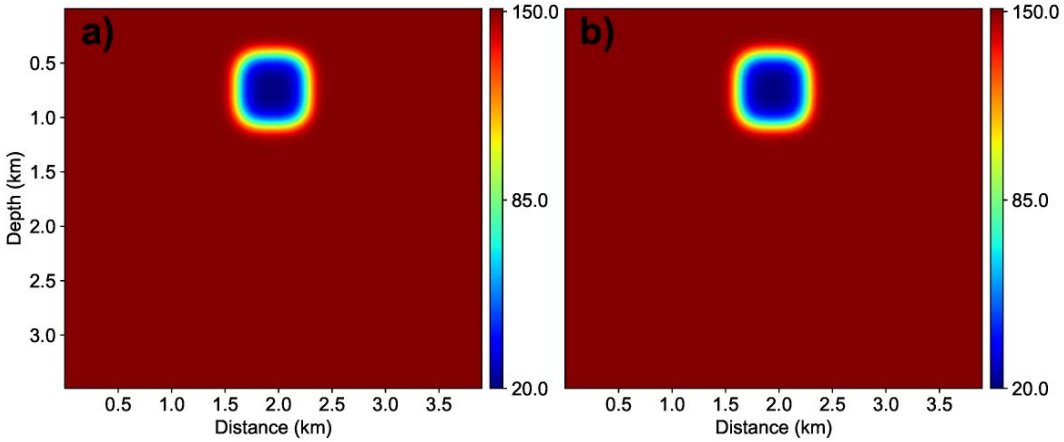

Figure 3: The true P-wave velocity quality factor Q_α model (a) and the true S-wave velocity quality factor Q_β model (b) used for testing our adaptive viscoelastic-waveform inversion method.

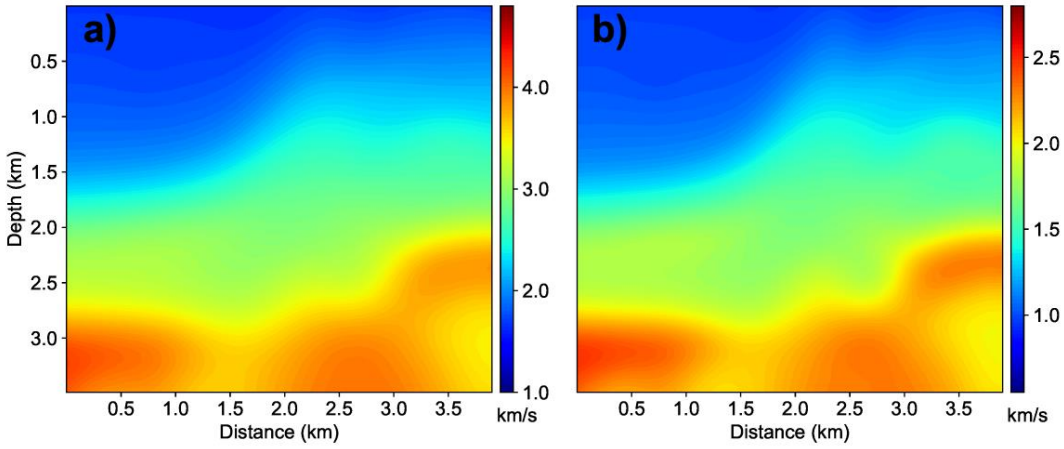

Figure 4: The initial P-wave velocity α model (a) and the initial S-wave velocity β model (b) used in adaptive viscoelastic-waveform inversion.

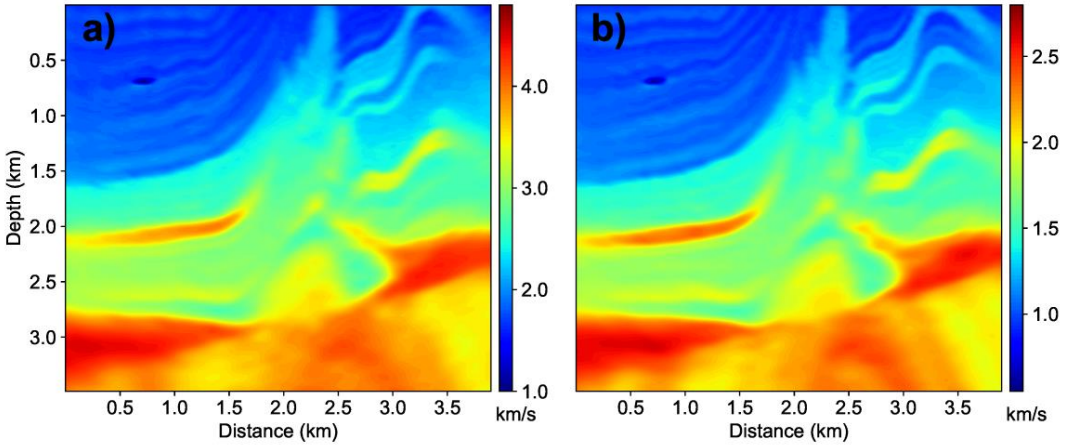

Figure 5: Inverted P-wave velocity α (a) and S-wave velocity β (b) models obtained in Stage I of adaptive viscoelastic-waveform inversion.

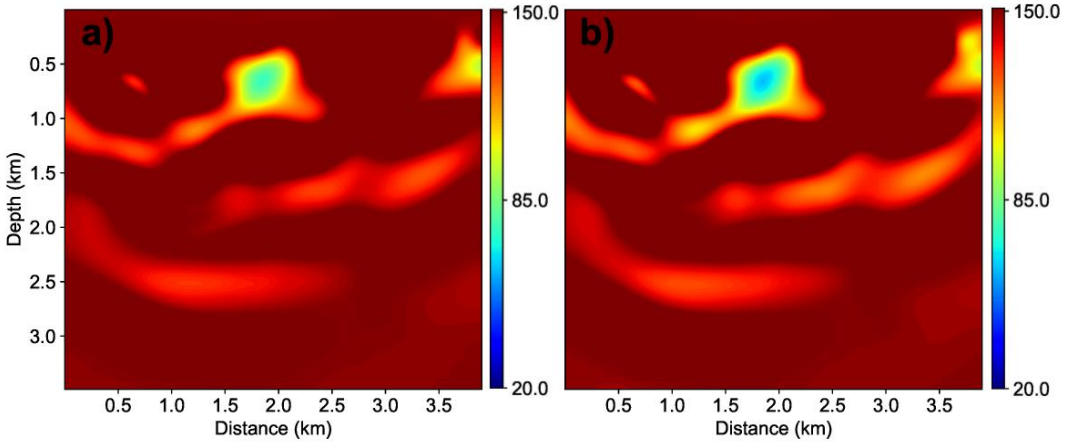

Figure 6: Inverted P-wave velocity quality factor Q_α (a) and S-wave velocity quality factor Q_β (b) using the conventional WD misfit function in Stage II of waveform inversion.

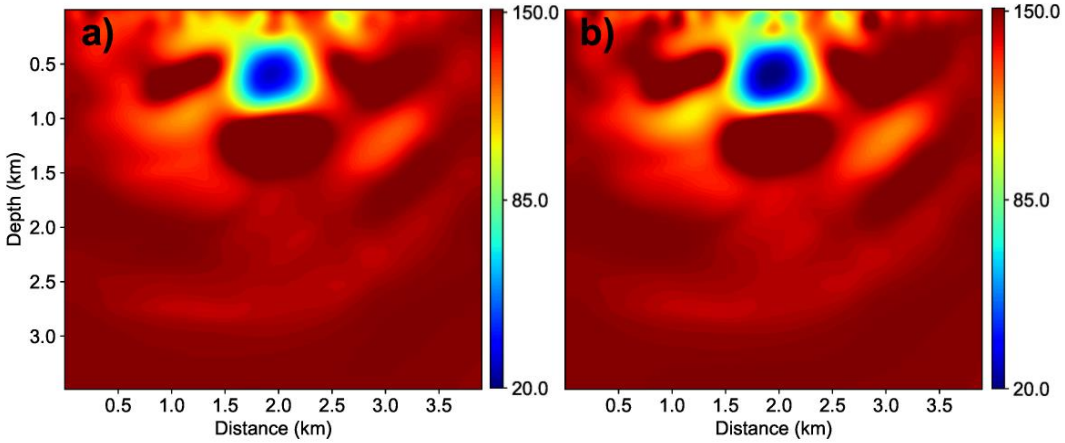

Figure 7: Inverted P-wave velocity quality factor Q_α (a) and S-wave velocity quality factor Q_β (b) using our adaptive viscoelastic-waveform inversion using the SAR misfit function and the local wavelet transform in Stage II of waveform inversion.

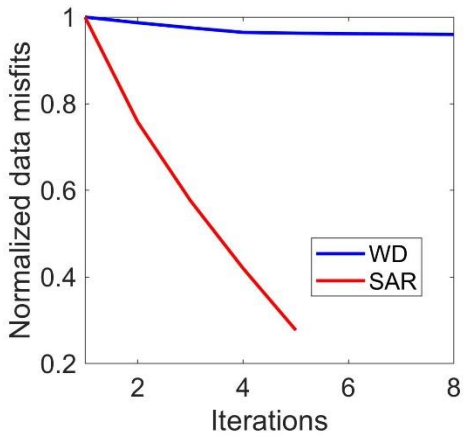

Figure 8: Data misfit reduction histories of WD and SAR misfit functions for attenuation inversion in Stage II.

3.2 Application of Adaptive Viscoelastic-Waveform Inversion to Seismic Data from the Blue Mountain Geothermal Field

Next, we apply our adaptive viscoelastic-waveform inversion method to the surface seismic data acquired at the Blue Mountain geothermal field. Figure 9 shows the seismic acquisition survey conducted in 2007. We apply our new method to seismic data along Line 3. The initial P-wave and S-wave velocity models are obtained using refraction tomography, as shown in Figure 10. The initial attenuation models are homogeneous with $Q_\alpha = Q_\beta = 150$.

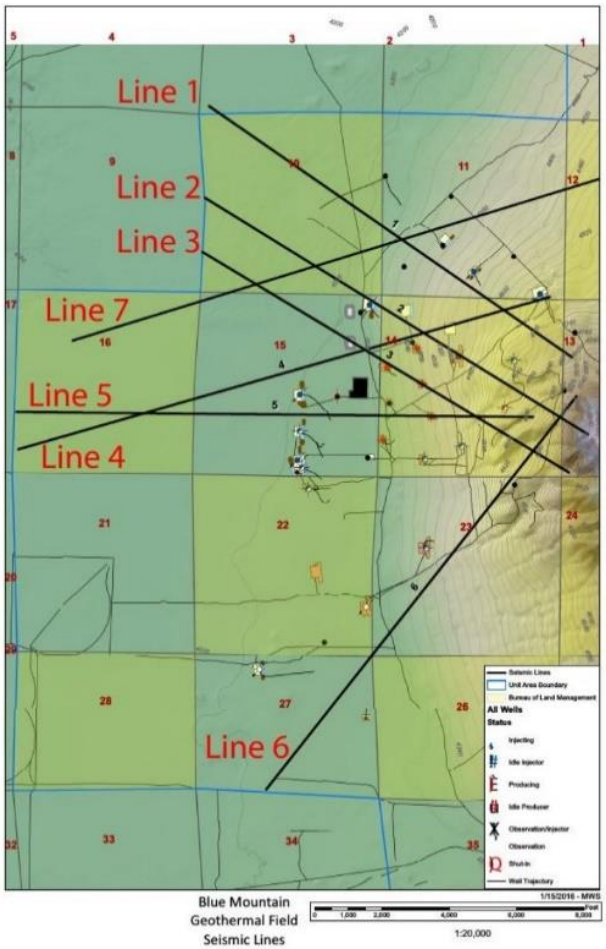

Figure 9: Surface seismic acquisition at the Blue Mountain geothermal field.

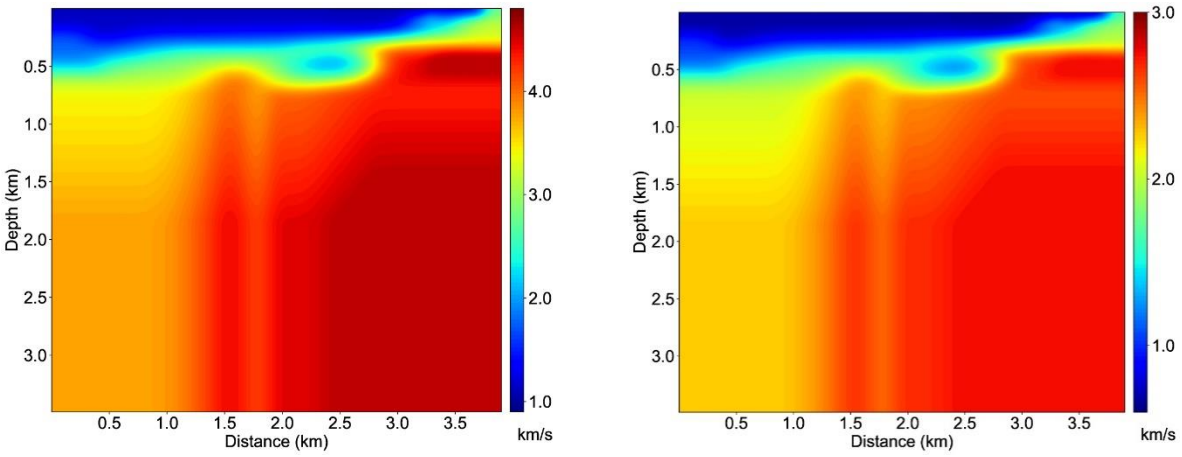

(a) (b)

Figure 10: The initial P-wave velocity α model (a) and S-wave velocity β model (b) yielded using refraction tomography.

Figure 11 shows the inverted P-wave and S-wave velocity models obtained in Stage I of our inversion with the WD misfit function. In Stage II, we use the SAR misfit function to invert for the attenuation models in Figure 12. In the shallow regions of the models (depths of 0-0.8 km), we obtain strong attenuation values, which are attributed to near-surface effects. More importantly, at the depths of 0.8-1.5 km, very strong attenuation anomalies ($Q_\alpha \approx 60$ and $Q_\beta \approx 40$) are reconstructed. The nearby injection and production wells are projected onto the inverted attenuation models, as indicated by the black and red lines in Figure 12. Positions of the injection and production wells are located on both sides of the attenuation anomalies, indicating that the inverted attenuation anomalies may be associated with the fluid-filled fracture/fault zones in the geothermal reservoirs at the Blue Mountain geothermal field.

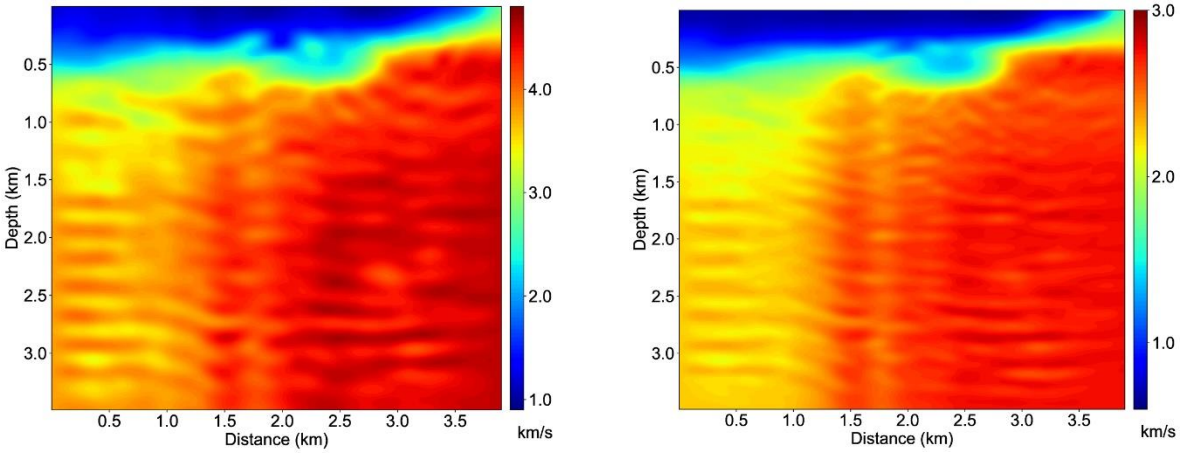

(b) (b)

Figure 11: The inverted P-wave velocity α model (a) and S-wave velocity β model (b) using the WD misfit function in Stage I of waveform inversion.

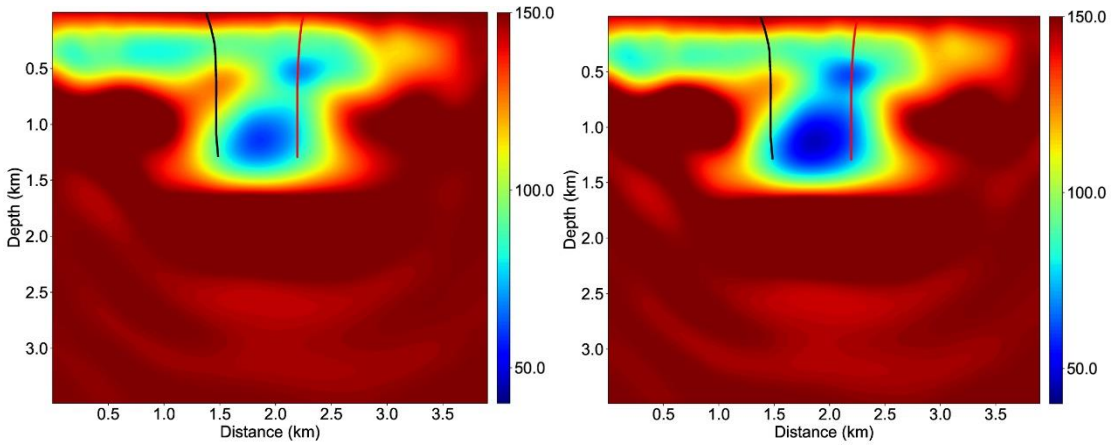

Figure 12: The inverted P-wave quality factor Q_α model (a) and S-wave quality factor Q_β model (b) using our adaptive viscoelastic-waveform inversion method.

4. CONCLUSIONS

We have developed a novel adaptive viscoelastic-waveform inversion method based on the local wavelet transform and spectral amplitude-ratio misfit function for inverting subsurface velocity and attenuation models. The synthetic example suggests that our new method is able to invert for both velocity and attenuation models reliably. We have applied our new method to a 2D line of surface seismic data acquired at the Blue Mountain geothermal field. Our results show very strong attenuation anomalies located between the nearby injection and productions wells, demonstrating that the regions with high-attenuation coefficients may be associated with geothermal reservoirs at the Blue Mountain geothermal field.

5. ACKNOWLEDGMENTS

This work was supported by the Geothermal Technologies Office (GTO) of the U.S. Department of Energy through contract DE-AC52-06NA25396 to Los Alamos National Laboratory (LANL). We thank AltaRock Energy Inc. for providing us with surface seismic data acquired at the Blue Mountain geothermal field, and thank Trenton Cladouhos of Cyrq Energy, Inc. for his support. This research used resources provided by the Los Alamos National Laboratory Institutional Computing Program, which is supported by the U.S. Department of Energy National Nuclear Security Administration under Contract No. 89233218CNA000001.

REFERENCES

Carcione, J. M., Kosloff, D., and Kosloff, R.: Viscoacoustic wave propagation simulation in the earth, *Geophysics*, **53**, (1988), 769-777.

Swyer, M., Uddenberg, M., Nordin, Y., Cladouhos, T., and Petty, S.: Improved Injection Strategies at Blue Mountain, Nevada Through an Improved Conceptual Model, Tracer Testing, and Injection-production Correlation, *Proceedings*: 41st Workshop on Geothermal Reservoir Engineering, Stanford, CA (2016).

Huang, L., Gao, K., Huang, Y., and Trenton, C.: Anisotropic Seismic Imaging and Inversion for Subsurface Characterization at the Blue Mountain Geothermal Field in Nevada, *Proceedings*: 43rd Workshop on Geothermal Reservoir Engineering, Stanford, CA (2018).

Optim Software and Data Solutions: Final Technical Report: Active Source Seismic Exploration and Development at the Blue Mountain Geothermal Project, Humboldt County, Nevada (2007).

Robertsson, A., Blanch, J., and Symes, W.: Viscoacoustic finite-difference modeling, *Geophysics*, **59**, (1994), 1444-1456.

Swyer, M., Uddenberg, M., Nordin, Y., Cladouhos, T., and Petty, S.: Improved Injection Strategies at Blue Mountain, Nevada Through an Improved Conceptual Model, Tracer Testing, and Injection-production Correlation, *Proceedings*: 41st Workshop on Geothermal Reservoir Engineering, Stanford, CA (2016).

Tarantola, A.: Inversion of seismic reflection data in the acoustic approximation, *Geophysics*, **49**, (1984), 1259-1266.

Virieux, J., and Operto, O.: An overview of full-waveform inversion in exploration geophysics, *Geophysics*, **74**, (2009), WCC1-WCC26.